Improvements in a Generic Approach to Low Level Data-Driven Segmentation Based on Separatrices

Shaadi Shidfar[1]
ss494@kent.ac.uk
Adina Ion[2]
k0843216@kingston.ac.uk
Lazaros Ktorides[1]
lariolaz@hotmail.com
Alan Colchester[1]
a.colchester@kent.ac.uk,www.kent.ac.uk/bio/colchester/

[1] Neurosciences and Medical Image Computing Group
University of Kent
Canterbury, UK

[2] Digital Imaging Research Centre
Kingston University
Kingston, UK

Abstract

Separatrices provide a promising generic approach for the first stages of data-driven segmentation. However, significant topological problems can arise when the approach is used with real, discretely sampled images, in particular through the incorrect detection of multiple adjacent saddles and when there are contacts between separatrices. To avoid the adjacent saddle problem we use a hexagonal grid. We analyse contacts systematically in a selection of 2-D images and identify the occurrence of separatrix crossings in a small number of these cases. We show that crossings generate invalid slope districts and propose an algorithm for their correction. We argue that correcting these will in turn improve the performance of graph simplification strategies for data-driven object detection.

1 Introduction

An important requirement in many image analysis applications, including medicine, is to be able to detect novel objects for which there is no satisfactory model, and also generation of graph-based data-driven descriptions of objects which can then be matched to high level models. Eigenvector-based segmentation method is an example of low level data driven segmentation which has been widely used [18, 20]. Graph-based image segmentation methods [19, 21] are other examples which generally represent the image as a graph G=(V,E) where V is a set of nodes representing image pixels and E is the set of edges connecting nodes on a certain similarity. In [4] a graph-based segmentation is proposed where unlike the previous similar methods, captures important non-local image properties in the image. This method assigns a weight to a boundary between two regions by comparing the intensity differences across the boundary and intensity difference between the neighbouring pixels in each region. The intensity difference across the boundary is relatively important if it is larger than the internal intensity differences of at least one of the regions.

Another powerful approach for extracting low-level image structure is based on separatrices [13]. The concepts originated from the classical work of Cayley [1] and Maxwell [11] who developed a framework for analysing terrain topography, and the terrain analogy is still very useful for understanding the processes in 2-D images, where image intensity is mapped to terrain height. Separatrices are defined algebraically as boundaries separating two modes of behaviour in a differential equation [10]. They run between critical points, namely local maxima, local minima and saddle points (Figure 1). A saddle in a 2-D image is characterised as a point where the gradient changes sign four times or more around the point. Starting from a saddle, a separatrix is a slope line or maximum gradient path (MGP), either uphill (uMGP) or downhill (dMGP), and continues until it ends at a maximum or minimum respectively. The network of separatrices forms the critical point configuration graph [13] (Figure 1). The smallest cells in this graph are called slope districts and their boundary critical points should always occur in a circular sequence as follows: {maximum - saddle1 - minimum - saddle2}; the starting point and direction are arbitrary and do not affect the definition.

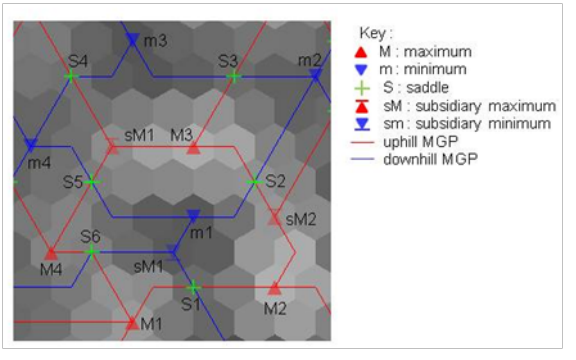

Figure 1: The critical point configuration graph of a hexagonal image cropped from a T2 weighted Brain MRI image. $G_1 = (V_1, E)$ where $V_1 = \{S2 - m2 - S3 - m3 - S4 - m4 - S5 - m1\}$ and E= {MGPs between each two adjacent nodes} surrounds a hill while $G_2 = (V_2, E)$ where $V_2 = \{S1 - M2 - S2 - M3 - S5 - M4 - S6 - M1\}$ surrounds a dale. $G_3 = G_1 \bigcap G_2 = \{S5 - m1 - S2 - M3\}$ surrounds the overlapping area between the hill and dale which is called a slope district.

Watershed segmentation methods have been widely used, e.g. [14] but it is not generally appreciated that watersheds and watercourses are separatrices, and the low points around a watershed , where water from one catchment area spills into another , are saddle points . The uMGPs running between the saddles and maxima are watershed lines which separate the watershed basins. The dMGPs are watercourse lines which divide the hills.

The separatrix methods have several strengths. They establish a low-level graph-based representation of the image at a very early stage of processing. This carries advantages for subsequent operations, for example when grouping to form larger objects [3]; detection of objects without needing to localise boundaries [6]; generating discrete alternative boundary representations for an object [7]; matching to high level symbolic models [9]; and ease of moving between two- and higher- dimensional image data and models.

However, the separatrix methods have various potential limitations. The issue of "over-

segmentation" is common to all low level methods if no prior assumptions are made about the size or smoothness of objects to be extracted. But a general purpose approach which can detect novel objects of unknown size must be able to extract small as well as large objects, so this apparent disadvantage is really a necessary feature in the design specification. The implication is that hierarchical grouping or multi-scale smoothing is required to extract the larger objects and simplify the image.

More importantly, there are significant methodological difficulties that arise when the approach is used with real, discretely sampled images. The definition of saddle points turns out to be non-trivial with discrete data [8]. Complex graph configurations can arise, some only in rare degenerate cases but others more commonly [13, 15]. These can interfere with the subsequent powerful graph simplification processes, and have limited further development of the methodology. Some of these problems have been discussed in previous publications [16] but a comprehensive analysis has been lacking.

Considering typical digital images sampled in a rectangular array, close examination of all closed paths within (4)-neighbour or (8)-neighbour pixel connectivity around critical points shows important topological inconsistencies [17]. This is illustrated in Figure 2 and figure 3. A tessellation which avoids these inconsistencies is given by a regular hexagonal grid.

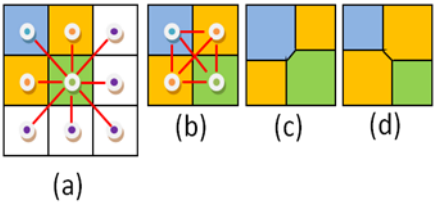

Figure 2: According to 8-neighbourhood pixel connectivity, blue and green pixels in (a) are neighbours. Adjacent objects should share a finite common edge which leads to (c) . This situation contradicts the 8-neighbourhood pixel connectivity because the yellow pixels should be neighbours and are not. The same situation happens in (d) where the yellow pixels share a common boundary in order to be neighbours.

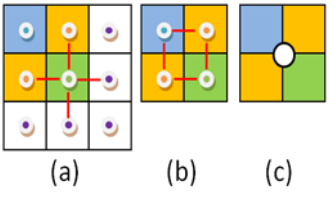

Figure 3: According to 4-neighbourhood connectivity the yellow nodes are neighbours of both the green and the blue node, but they are not themselves neighbours. Similarly the blue and green nodes are not neighbours. The only way this can happen in the real world is existence of an implied object as in (c). This issue causes unresolved topological neighbourhood conflicts.

There are hardware and software methods for converting square lattices to hexagons. Different software schemes have been proposed. For example Hartman [8] used a hexagonal grid on triangular pixels. Each two vertically adjacent square pixels were averaged to create a triangle. Each hexagon was then created from 24 triangles or 48 square pixels. Brick walls are an easy approximation of hexagonal lattice where pixels in alternative rows are shifted by half a pixel to simulate the hexagonal lattice. Fitz and Green [5] used this approach. They first subsampled the image such that each sampled image pixel was consisted of four original pixels. They then shifted alternative sampled rows by half a pixel. Her [9] created a new grid by starting from a rectangular grid and combining every two adjacent pixels consecutively along a specified axial direction of the image. A detailed survey on this topic can be found in [12].

One of the important types of special events that can complicate the construction and interpretation of the critical point configuration graph (CPCG) occurs when an MGP contacts another MGP (excluding the natural events at the saddles which generate the MGPs and terminations at extrema). We analyse MGP contacts systematically in a selection of 2-D images, in order to establish a more stable framework for 2-D and 3-D data-driven segmentation in future work.

2 Methods

The first processing stage is to convert rectangular pixels to hexagonal pixels (Figure 1), using an upsampling and then resampling strategy with a scaling factor which generates approximately the same number of hexagons as the original rectangles and preserves the full resolution of the original image. The hexagons are overlaid on the upsampled pixels and the intensity value for each hexagonal pixel is defined as the average of the grey values of the square sub-pixels belonging to that hexagon. Hexagonal lattice avoids the problems described by Fu [6] in saddle detection with rectangular pixels, which have topologically inconsistent neighbourhoods.

The hexagons guarantee a complete neighbourhood where all neighbours share a common edge and not just a vertex. We then construct an object-based data structure where the neighbours are listed in an anticlockwise sequence. Local maxima and minima are defined by having neighbours that are all of lower or of higher intensity respectively, which is the same as saying that there are no sign changes between downhill or uphills in the cyclic list. Most points are standard "hillside" points (we will continue to use the convenient terrain analogies) which have two sign changes. Saddles are defined as having four (commonly), or (rarely) six, sign changes.

From every saddle, maximum gradient paths (MGPs) are generated. In each uphill neighbourhood sector of the saddle, the neighbour with the highest intensity is linked; this process is repeated until a maximum is reached: this grows an uphill MGP (uMGP). Downhill MGPs (dMGPs) are grown in the same way. Thus, for standard saddles with four sign changes and four sectors, the cyclic sequence of paths generated will be {uMGP - dMGP - uMGP - dMGP}.

The critical point configuration graph is constructed by linking the critical points (nodes) and the MGPs (edges). Slope districts are closed loops or cells in this graph (Figure 1) and should have the cyclic boundary sequence {saddle1 - uMGP - maximum - uMGP - saddle2 - dMGP - minimum - dMGP - saddle1}, i.e. four critical points (the nodes) linked by four MGPs (the edges). The list is reversible and the starting point is arbitrary. In our test images

we constructed closed loops of all critical points and their linking MGPs, and in each case tested if these formed valid slope districts.

Excluding the terminations of MGPs, we detect all instances where two MGPs can make contact (i.e. they share a common hexagon). At contact points we analysed the immediate hexagon neighbourhood and also the neighbourhood in the CPCG. We excluded plateaus in this analysis and restricted the processing to regions of interest away from the image borders. We used images from four sources for these experiments: MRI of the brain; MRI with added noise; x-ray angiography; micrograph of a blood film; and an image of a changing texture pattern (Figure 4).

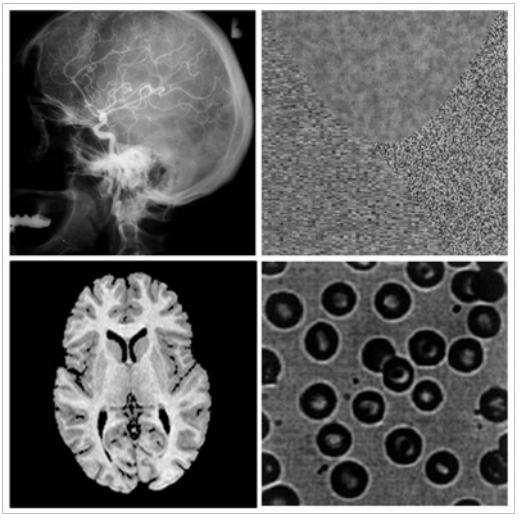

Figure 4: Clockwise from the top left image; x-ray angiography; image of a changing texture pattern; micrograph of a blood film; MRI of the brain

3 Results

We analysed regions of interest from the images shown in Figure 4, ranging in size from 539 to 1346 pixels (Figure 5). For a given image size, the numbers of critical points, MGPs and slope districts naturally depend on the structure of the image, with smooth images having a small number, and images with many small objects or noise larger numbers (Table 1, Table 2). The addition of noise increases the number of critical points, MGPs and slope districts (Figures 5(a) and 5(b)). The number of maxima does not have to be equal to the number of minima. However, the Euler number which is the sum of the saddles plus 2 should be equal to the sum of the maxima and minima. In a small region of interest this does not hold exactly, but the differences in our examples amounted only to a few percent (Table 1). In contrast, in 4-neighbourhood and 8-neighbourhood square pixels number of saddles was underestimated and overestimated. Tables1, 3 and 4 illustrate expected saddles using Euler formula (maxima+ minima = saddles + 2) and number of saddles detected within each image.

Slope district statistics are given in Table 2. While the majority of cycles formed valid slope districts, in every image there were instances of invalid slope districts (about 10% of

Type of point (6 neighbourhood connectivity)	Brain MRI	Brain MRI, noise added	X-ray angiogram	Blood film micrograph	Synthetic texture pattern
Pixels/hexagons	539	539	1712	1080	1346
Maxima	33	45	33	46	51
Minima	16	37	34	52	56
Max + Min (M)	49	82	67	98	107
Saddles (S)	47	80	70	100	106
Euler number (E =S+2)	49	82	72	102	108
Excess of M over E (%)	0%	0%	-7%	-4%	-1%
Saddles over (M-2) (%)	100%	100%	108%	104%	101%

Table 1: Pixels and critical points in the regions of interests (Figure 5) calculated using 6 neighbourhood. Cells show numbers of points unless otherwise stated.

the total). The commonest type of contact event was when alike MGPs (i.e. both uMGP or both dMGP) merge before continuing to their extremum. These merge points, which we term subsidiary Maxima or minima (Figure 1 symbols "sM" and "sm"), are normal events. In our examples these occurred with a frequency of around 50 - 100% of the saddles. In no case did they generate invalid slope districts.

Unalike MGP contacts (i.e. between one uMGP and one dMGP) were also seen in all images (Table 2), with a frequency of 2-6% of MGPs. Kissings (Figure 6, marked "K" on the image), where two unalike MGPs touch but then separate without crossing, comprise about half of the unalike contacts. Kissings do not lead to invalid slope districts. Crossings form the other category of unalike contacts and occur with a similar frequency to kissings. In contrast to all other types of contact, in every case crossing MGPs lead to CPCG cycles which are not valid slope districts.

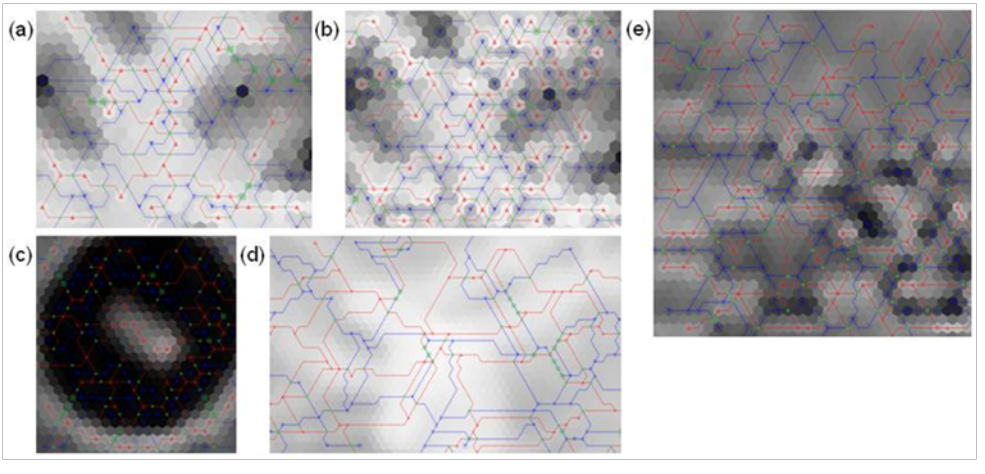

Figure 5: Regions of interest cropped from images in Figure 4. (a) from brain MRI; (b) from brain MRI with added noise; (c) from micrograph of blood film; (d) from x-ray angiogram; (e) from image of a changing texture pattern.

Type of path, contact events and districts	Brain MRI	Brain MRI, noise added	X-ray angiogram	Blood film micrograph	Synthetic texture pattern
MGPs not ending at the border	167	290	237	239	383
Contacts (all)	45	70	76	59	89
Like-MGP contacts (subsidiary extrema)	38	65	66	45	82
Like-MGP contacts as % of MGPs	23%	22%	28%	19%	21%
Unalike MGP contacts	7	5	10	17	7
Kissings	4	2	8	5	4
Kissings as % of MGPs	2%	1%	3%	2%	1%
Crossings	3	3	2	12	3
Crossings as % of MGPs	2%	1%	1%	5%	1%
Non border SloDs	73	134	114	115	186
Valid SloDs	68	129	108	108	178
Invalid SloDs	5	6	7	9	12

Table 2: Paths, contact events and districts in the regions of interest (Figure 5) calculated using 6 neighbourhood

Type of point (8 neighbourhood connectivity)	Brain MRI	Brain MRI, noise added	X-ray angiogram	Blood film micrograph	Synthetic texture pattern
Pixels	567	567	1798	1122	1406
Maxima	36	51	40	50	64
Minima	27	49	36	54	63
Max + Min (M)	63	82	76	69	127
Saddles	92	159	116	156	186
Euler number (E =S+2)	94	161	118	158	188
Excess of M over E (%)	-33%	-49%	-36%	-56%	-32%
Saddles over (M-2) (%)	150%	200%	150%	230%	150%

Table 3: Number of critical points calculated using 8 neighbourhood square pixels. Same regions of interest as used for table 1 has been used.

Type of point (4neighbourhood connectivity)	Brain MRI	Brain MRI, noise added	X-ray angiogram	Blood film micrograph	Synthetic texture pattern
Pixels	567	567	1798	1122	1406
Maxima	46	88	54	69	87
Minima	42	79	52	62	76
Max + Min (M)	88	167	106	131	163
Saddles	21	21	27	42	51
Euler number (E =S+2)	23	23	29	44	53
Excess of M over E (%)	198%	626%	265%	198%	207%
Saddles over (M-2) (%)	24%	13%	26%	33%	32%

Table 4: Number of critical points calculated using 4 neighbourhood square pixels. Same regions of interest as used for table 1 has been used.

We analysed all crossing events in detail. Figure 6(i) is an example which illustrates the conclusions. A crossing point can always be identified by the list of MGPs entering and leaving the point. The list must be in order of radial position, and is cyclic (last MGP is next to the first). We identify an MGP by the id of its start and end points. Thus, for the crossing point X1 in Figure 6(i), the list (anticlockwise) reads {S1>M1 - S3>m1 - S1>M1 - S3>m1}. Note that each id appears twice because each path enters and leaves the point. If there were no crossing, the list would read {S1>M1 - S1>M1 - S3>m1 - S3>m1}. To resolve the crossing we propose to divert one (but not both) of the MGPs at the crossing. This means that there are two options for resolving the crossing. Option 1 (Figure 6(ii)): The dMGP S3>m1 is preserved but the uMGP S1>M1 is diverted at X1 and runs as a normal MGP to M2, creating the revised MGP S1>M2. The original path S1>X1 is still used, but X1>M1 is suppressed. Option 2 (Figure 6(iii)): The uMGP S1>M1 is preserved but the dMGP S3>m1 is diverted at X1 and then runs as a normal MGP to m2, creating the revised MGP S3>m2. The original path S3>X1 is still used, but X1>m1 is suppressed.

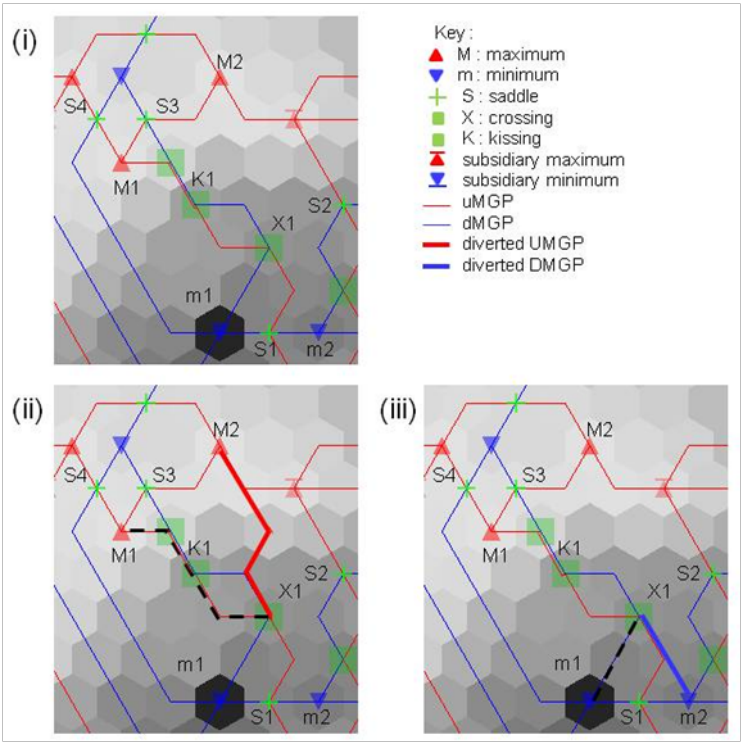

Figure 6: The CPCG of the neighbourhood of a crossing (X1). In (i) {S1 - m2 - S2 - M2 - S3 - m1 - S1} and {S3 - M1 - S4 - m1 - S1- M1 - S4 - m1 - S3} are two of the incorrect slope districts in this region. (ii) and (iii) show two options of solving the problem, one by preserving the dMGP and diverting the uMGP and another by preserving the uMGP and diverting the dM

One crossing is associated with two or more complex CPCG cycles which break all the rules for a valid slope district. For each crossing we identify the union of the invalid

Option no	Saddle S1 connected to :	Saddle S3 connected to:	Figure	Evaluation from cyclic list of boundary critical points
Original	M1	m1	Figure 4(i)	Invalid: in anticlockwise cyclic list S3 lies between S1 and M1, while m1 lies between M1 and S1
Resolution: option 1	M2	m1	Figure 4(ii)	Possible: in anticlockwise cyclic list both S3 and m1 lie between M2 and S1
Resolution: option 2	M1	m2	Figure 4(iii)	Possible: in anticlockwise cyclic list, S3 and m2 lie between S1 and M1
Invalid option 3	M2	m2	-	Invalid: in anticlockwise cyclic list S3 lies between M2 and S1,while m2 lies between S1 and M2

Table 5: Number of critical points calculated using 4 neighbourhood square pixels. Same regions of interest as used for table 1 has been used.

slope districts, which gives the boundary of the valid graph elements in the surrounding neighbourhood. In Figure 6 this boundary is the graph cycle {m1 - S1 - m2 - S2 - M2 - S3 - M1 - S4}. Analysis of the paths which must enter the invalid zone, and the possible critical points to which they could in principle be connected when they terminate at the boundary of the zone (Table 5), provides an "inward looking" view of path crossings complementary to the "outward looking" view from the contact point. As shown in the Table, two possible valid connections are identified if paths are redirected. Note that these solutions are the same as those derived from the path connections at the contact point.

4 Discussion

In order to create accurate separatrices and thus accurate slope districts the fundamental concepts need to be correct. Redundant saddles will cause redundant separatrices and redundant overlapping slope districts resulting in over-segmentation of the image. Using rectangular pixels with an 8-neighbours (Table 3), the frequency of saddles in the image is 150% - 230% more than what we expect using the Euler formula (maxima+ minima = saddles + 2). When checked with rectangular pixels and 4-neighbours there were 13 to 33% fewer saddles than expected using Euler formula (Table 4). In contrast to these over- and under-estimates, with hexagonal pixels the saddle frequency was very close to the Euler prediction (Table 1). Considering that we excluded image border pixels from our calculations the minor differences can be ignored. As evaluated by the Euler criterion and by inspection of example images, the hexagons appeared almost completely to avoid the recognised "multiple saddle point problem" [6] arising with 8-neighbour rectangular pixels in the discrete domain.

We also explored the contacts in each image. As expected, contacts between maximum gradient paths were common in all our images. The majority were subsidiary maxima or minima, where two or more alike MGPs (i.e. both uMGPs or both dMGPs) merge before

reaching an extremum. These are a normal event in the CPCG and are generally easy to interpret. Most of the other kinds of contacts were also found to be valid, despite initial inspection sometimes suggesting (for example at kissing points) an error in processing or an inconsistency between the definitions of the point/ path/ district definitions.

The one invalid contact event was the crossing of unalike MGPs. This violates the basic topology rules, not only at the crossing and through the expected "twisted" slope district, but by generating a set of complex topological conflicts in adjacent slope districts. Analysis of the immediate neighbourhood of a crossing showed that this is a degenerate event; a very small change in intensities would avoid the crossing, which would divert one of the outbound paths so that the crossing does not occur. This suggests one possible algorithm to resolve crossings, namely to perturb the local intensities in such a way that the crossing would not occur. However, we preferred not to modify the raw data: our proposed algorithm, which we have not yet implemented, involves diverting one of the crossing paths, effectively converting the crossing into a kissing (Figure 6 and Table 5). Choosing which path to divert could be based on local geometry or overall slope district properties, or could be arbitrary.

We presented this algorithm initially from the outward-looking perspective of the local neighbourhood of the crossing point. It was of particular interest to establish that essentially the same algorithm can be formulated from the inward-looking perspective of the (valid parts of the) CPCG surrounding encircling the zone of the crossing. Topological rules applied to the cyclic list of critical points around the boundary of the union of the invalid districts showed unequivocally that there had to be a crossing within this unified district, regardless of the exact location of that crossing, i.e. crossings can be detected "remotely" by analysis of the CPCG (Table 5, row 1). Similarly, these topological rules could be used to generate the possible valid connections across the unified district between critical points on the boundary. This remote approach generated the same basic solution options as the local approach. Furthermore, it became clear that the detailed topological rules applied to the cyclic-list-ordering of paths leaving the crossing towards the periphery were the same as those applied to the cyclic-list-ordering of paths leaving the periphery towards the middle of the unified region.

Our demonstration that most of the contact events between MGPs are consistent with all of the definitions of data elements in the CPCG provides further support of the generality of separatrix-based approach used with discrete images. However, contacts between MGPs that lead to crossings do occur to corrupt the graph. Correcting these will in turn correct some inconsistent results in graph simplification strategies for data-driven object detection, which we believe will lead to significant improvements in applications of these techniques to a wide range of biomedical and other image types.

References

[1] A. Cayley. On contour and slope lines. *The London, Edinburgh and Dublin Philosophical Magazine and Journal of Science*, 18:264–268, 1859.

[2] J. H. Connell and J. M. Brady. Generating and generalizing models of visual objects. *Artificial Intelligence*, 31:159–183, 1987.

[3] M. A. G. de Carvalho, R. A. Lotufo, and M. Couprie. Morphological segmentation of yeast by image analysis. *Image and Vision Computing*, 25(1):34–39, 2007.

[4] P. F. Felzenszwalb and D. P. Huttenlocher. Efficient graph-based image segmentation. *International Journal of Computer Vision*, 59(2):167–181, 2004.

[5] AP Fitz and RJ Green. Fingerprint classification using a hexagonal fast fourier transform. *Pattern Recognition*, 29(10):1587–1597, 1996.

[6] G. Fu, S. A. Hojjat, and A. C. F. Colchester. Integrating watersheds and critical point analysis for object detection in discrete 2d images. *Medical image analysis*, 8:177–185, 2004.

[7] L. D. Griffin, A. C. F. Colchester, G. P. Robinson, and D. J. Hawkes. *Structure sensitive scale and the hierarchical segmentation of grey-level images*, pages 24–32. Proceedings of Visualization in Biomedical Computing (VBC '92). SPIE, Washington, -32676 1992.

[8] N. P. Hartman and S. L. Tanimoto. A hexagonal pyramid data structure for image processing. *IEEE transactions on systems, man, and cybernetics*, 14(2):247–256, 1984.

[9] I. Her and C. T. Yuan. Resampling on a pseudohexagonal grid. *CVGIP: Graphical Models and Image Processing*, 56(4):336–347, 1994.

[10] E. A. Leontovich. The creation of limit cycles from a separatrix. *Sov.Math.Daklady*, 4: 641–644, 1951.

[11] J. C. Maxwell. *The scientific papers of James Clerk Maxwell. Vol II: On Hills and Dales*. Cambridge University Press, Cambridge, -32676 1890.

[12] L. Middleton and J. Sivaswamy. *Hexagonal image processing: a practical approach*. Springer-Verlag New York Inc, 2005.

[13] L. R. Nackman. Two-dimensional critical point configuration graphs. *IEEE Transactions on Pattern Analysis and Machine Intelligence*, 6(4):442–450, 1984.

[14] K. Parvati, B. S. P. Rao, and M. M. Das. Image segmentation using gray-scale morphology and marker-controlled watershed transformation. *Discrete Dynamics in Nature and Society*, 2008, 2009.

[15] P. L. Rosin. Early image representation by slope districts. *Journal of Visual Communication and Image Representation*, 6(3):228–243, 1995.

[16] P. L. Rosin, A. C. F. Colchester, and D. J. Hawkes. Early image representation using regions defined by maximum gradient paths between singular points. *Pattern Recognition*, 7:695–711, 1992.

[17] P. J. Scott. An algorithm to extract critical points from lattice height data. *International Journal of Machine Tools and Manufacture*, 41(13-14):1889–1897, 2001.

[18] J. Shi and J. Malik. Normalized cuts and image segmentation. *IEEE Transactions on Pattern Analysis and Machine Intelligence*, 22(8):888–905, 2000.

[19] R. Urquart. Graph theoretical clustering based on limited neighbourhood sets. *Pattern Recognition*, 15 No. 3.:173–187, 1982.

[20] Y. Weiss. Segmentation using eigenvectors: a unifying view. In *iccv*, page 975. Published by the IEEE Computer Society, 1999.

[21] C. T. Zahn. Graph-theoretical methods for detecting and describing gestalt clusters. *IEEE Transactions on Computers*, C-20 No. 1:68–86, 1971.